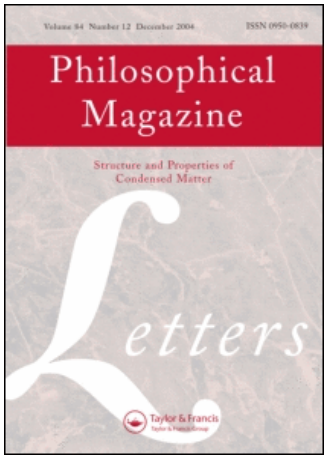


Philosophical Magazine Letters
Publication details, including instructions for authors and subscription information:
http://www.informaworld.com/smpp/title~content=t713695410

# Microstructural and magnetic properties of bulk $La_{1-x}Pr_xMnO_{3\,\delta}$ (x = 0.2, 0.3, 0.5)

To link to this article: DOI: 10.1080/09500830601120450
URL: http://dx.doi.org/10.1080/09500830601120450

*Philosophical Magazine Letters*,
Vol. 87, No. 2, February 2007, 75–83

Taylor & Francis
Taylor & Francis Group

# Microstructural and magnetic properties of bulk $La_{1-x}Pr_xMnO_{3+\delta}$ ($x = 0.2, 0.3, 0.5$)

Y. L. ZHU*

Shenyang National Laboratory for Materials Science, Institute of Metal Research, Chinese Academy of Sciences, Shenyang 110016, China

(*Received 7 July 2006; in final form 2 November 2006*)

The magnetic, structural and microstructural properties of bulk $La_{1-x}Pr_xMnO_{3+\delta}$ have been studied as a function of Pr doping. Magnetization versus temperature measurements show that $La_{0.8}Pr_{0.2}MnO_{3+\delta}$ undergoes one magnetic transition, while $La_{0.7}Pr_{0.3}MnO_{3+\delta}$ and $La_{0.5}Pr_{0.5}MnO_{3+\delta}$ exhibit two magnetic transitions. X-ray diffraction and transmission electron microscopy studies indicate that all these compounds share an orthorhombic structure, which is derived from and also closely related to the ideal perovskite structure. Besides physical properties, the salient contrast between microstructures in these compounds is that there are high-density oriented microdomains in $La_{0.8}Pr_{0.2}MnO_{3+\delta}$, whereas $La_{0.7}Pr_{0.3}MnO_{3+\delta}$ and $La_{0.5}Pr_{0.5}MnO_{3+\delta}$ are free of these microstructural characteristics. A possible mechanism of domain formation is discussed.



## 1. Introduction

The observation of colossal magnetoresistance (CMR) in manganese oxides crystallizing in the perovskite structures has generated considerable interest in the physical properties of this class of compounds, particularly the interplay of structure, microstructure, and magnetism. Colossal magnetoresistance has been reported in $La_{1-x}A_xMnO_3$ (A = Ca, Sr, Ba, Ce) [1–5], $Pr_{1-x}Ca_xMnO_3$ [6, 7] and $Pr_{1-x}Sr_xMnO_3$ [8]. A review paper by Rao *et al*. [9] discusses in detail giant magnetoresistance, charge ordering and other novel properties in these manganates. From the viewpoint of crystallography, three structural polymorphs in these CMR oxides were identified [10], namely rhombohedral ($R\bar{3}c$), orthorhombic (*Pnma*), and monoclinic ($P2_1/c$). All these phases have slightly deformed perovskite structure owing to the distortion of the $MnO_6$ octahedra. Furthermore, microstructural characteristics in thin films of these oxides are generally recognized to be domain-oriented [11–14], no matter whether the crystal is orthorhombic or rhombohedral. It was also reported that the crystallographic domain orientation might play a very important role in getting magnetic anisotropy [15].

In the past few years, the magnetic and electronic phase diagrams of several manganites have been established as a function of doping $x$. For Sr substitution, Tokura and collaborators [16] have established the phase behaviours with

*Email: ylzhu@imr.ac.cn

*Philosophical Magazine Letters*
ISSN 0950-0839 print/ISSN 1362-3036 online © 2007 Taylor & Francis
http://www.tandf.co.uk/journals
DOI: 10.1080/09500830601120450

Sr doping level. They found that at low temperatures, the $La_{1-x}Sr_xMnO_3$ crystals for $0.1 < x < 0.5$ are ferromagnetic. The phase diagram mapped out by Tomioka *et al.* [7] for $Pr_{1-x}Ca_xMnO_3$ ($x < 0.5$) showed that at low temperature, the $Pr_{1-x}Ca_xMnO_3$ crystals become ferromagnetic for $0.15 < x < 0.3$, but antiferromagnetic for $0.3 < x < 0.5$. These findings indicate that, in a certain range of doping, the magnetic properties are closely related with doping $x$. According to our previous studies [14], the structure and microstructure of the CMR oxides, whether in thin films or bulk, are related to the doping level $x$. Therefore, there must be a link between microstructure and magnetic properties in these oxides, which is worthwhile to establish for all the CMR oxides.

Recently, a manganite $La_{0.7}Pr_{0.3}MnO_3$ in which the rare-earth element La was substituted by the rare-earth element Pr has been investigated and found to be an electron-doped compound exhibiting CMR after annealing in a flowing argon atmosphere [17], although the samples sintered in air without any further annealing treatment do not show a discernable metal–insulator transition and CMR. In this paper, we focus on the relationships between Pr doping, structure, microstructure and magnetic properties of as-sintered bulk $La_{1-x}Pr_xMnO_{3+\delta}$ with $x = 0.2$, 0.3 and 0.5. The relationships between these parameters have been established.



## 2. *Experimental procedures*

The $La_{1-x}Pr_xMnO_{3+\delta}$ (LPMO) series ($x = 0.2$, 0.3, 0.5) were prepared by a standard ceramic-sintering process in air. Stoichiometric mixtures of high-purity $La_2O_3$, $Pr_6O_{11}$ and $MnCO_3$ powders were pre-sintered at 1073 K for 12 h. Then, the powders were pressed into bars and calcined at 1203 K for 24 h, 1373 K for 24 h and 1473 K for 12 h, respectively. The as-received bars were scraped, ground and pressed after each heating. At the final stage the bars were sintered at 1573 K for 12 h and furnace cooled to room temperature.

Magnetization was measured using a Quantum Design superconducting quantum interference device (SQUID) in the temperature range 1.7–350 K. X-ray diffraction (XRD) data were collected from 20° to 70° using Cu K$\alpha$ radiation. Specimens for TEM observation were prepared by a conventional method; namely slicing, grinding, dimpling and finally ion-milling. A JEOL 2010 high-resolution electron microscope (HREM), with point resolution of 0.194 nm and working at 200 kV, was used to carry out contrast analysis and lattice imaging.

## 3. Results and discussion

### 3.1. *Magnetic properties of the $La_{1-x}Pr_xMnO_{3+\delta}$ series*

The magnetization curves for the three compositions of LPMO measured during cooling at a magnetic field of $H = 100$ Oe are shown in figure 1. The curves indicate a nearly constant value of $T_c$ for bulk $La_{0.8}Pr_{0.2}MnO_{3+\delta}$, $La_{0.7}Pr_{0.3}MnO_{3+\delta}$ and $La_{0.5}Pr_{0.5}MnO_{3+\delta}$, which is in contrast with the $T_c$ dependence on the doping level $x$ in the $La_{1-x}Sr_xMnO_3$ system [16]. From figure 1, it is also seen that

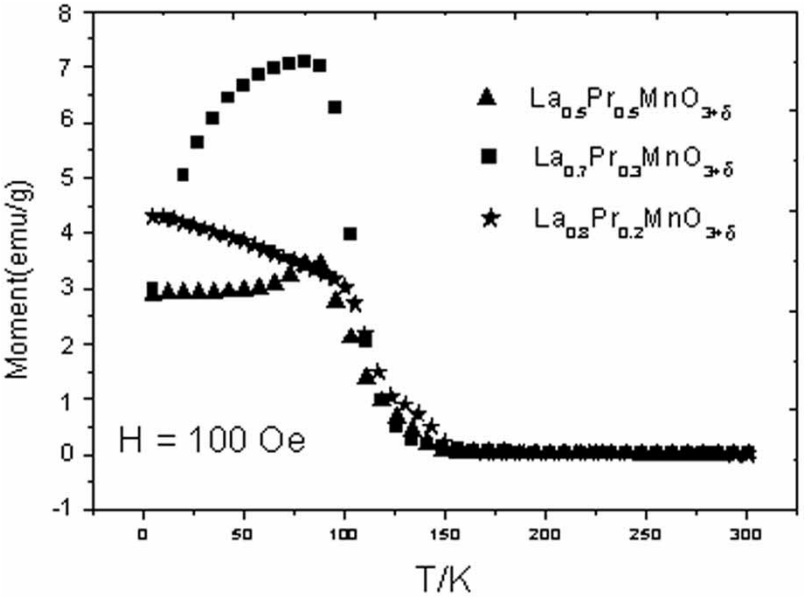


Figure 1. Temperature dependence of the magnetization of bulk $La_{1-x}Pr_xMnO_{3+\delta}$ ($x = 0.2, 0.3, 0.5$).

$La_{0.8}Pr_{0.2}MnO_{3+\delta}$ shows a different magnetic behaviour compared with the LPMO compounds for $x = 0.3$ and 0.5. It seems that with decreasing level of Pr doping, the ferro- to antiferromagnetic (FE–AFE) transition is suppressed and $T_N$ moves to a lower temperature. In fact, undoped $LaMnO_3$ is an antiferromagnetic phase [6] and another end member of $PrMnO_3$ is also antiferromagnetic at room temperature [18]. When doped with rare-earth Pr to substitute for the similar rare-earth element La, it is generally believed that Pr-doped $LaMnO_3$ should retain the antiferromagnetic state for all doping levels [19]. Therefore, the magnetic curve of $La_{0.8}Pr_{0.2}MnO_{3+\delta}$ is of interest and worthy of further investigation. It may result from wall pinning due to some inhomogeneity or defects in the magnetic walls. Investigations on structures and microstructures of the LPMO series are a necessary step to correlate structure-property in these manganites.

### 3.2. *X-ray diffraction patterns of the $La_{1-x}Pr_xMnO_{3+\delta}$ series*

Figures 2a–c are X-ray diffraction patterns of the $La_{1-x}Pr_xMnO_{3+\delta}$ series for $x = 0.2$, $x = 0.3$ and $x = 0.5$, respectively, at room temperature. The three compositional LPMO samples are all single phase, indicating that the mixtures of starting materials were fully reacted during the solid reaction process. All these patterns can be indexed on the basis of the orthorhombic lattice with lattice parameters of $a_o \approx a_p 2^{1/2} = 0.54$ nm, $b_o \approx 2a_p = 0.77$ nm, $c_o \approx a_p 2^{1/2} = 0.54$ nm, where $a_p$ is the lattice parameter of an ideal cubic perovskite structure, namely 0.39 nm. In a previous study on $La_{1-x}Sr_xMnO_3$, it was found that the lattice type is related to the

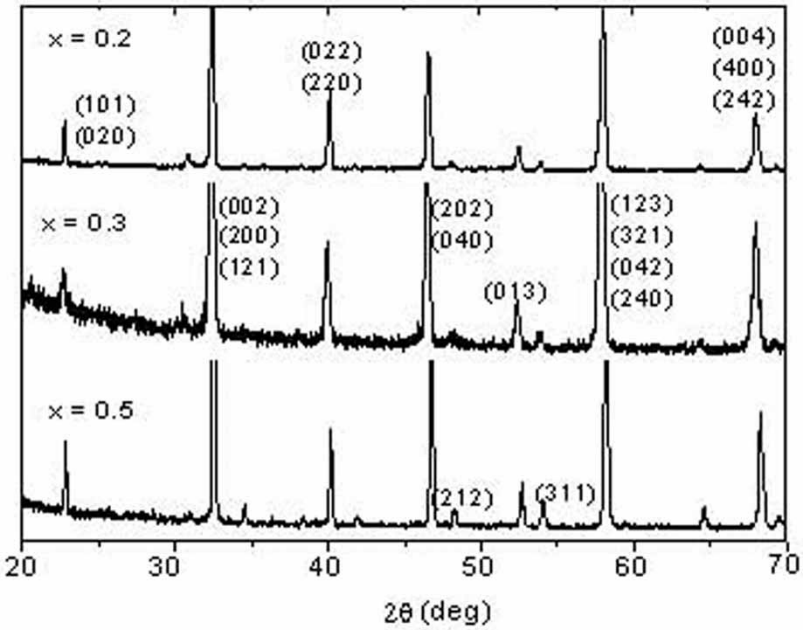


Figure 2. X-ray diffraction patterns of bulk $La_{1-x}Pr_xMnO_{3+\delta}$ ($x = 0.2, 0.3, 0.5$). All these patterns can be indexed on the basis of the orthorhombic structure with $a_o \approx 0.54$ nm, $b_o \approx 0.77$ nm, $c_o \approx 0.54$ nm.

doping level. For instance, $La_{1-x}Sr_xMnO_3$ has an orthorhombic structure at room temperature when $x < 0.175$; but a rhombic structure when $x > 0.25$; when $0.175 < x < 0.25$, it changes from orthorhombic to rhombic on increasing the temperature [15]. $La_{1-x}Ca_xMnO_3$ also shows a similar structural transition with changing $x$ [20]. The driving force arises mainly from the difference in the ionic radii of $La^{3+}$ and $Sr^{2+}$, and $La^{3+}$ and $Ca^{2+}$, and has little to do with the doping level itself, as stated by Tokura [21]. That the as-received $La_{1-x}Pr_xMnO_{3+\delta}$ compounds in the present study keep the same lattice structure over a widely ranged doping level might result from the similar physical characteristics of the cation ions Pr and La, both of which belong to the La series of rare-earth elements. Detailed investigation indicates that when $x$ increases from 0.2 to 0.3, the positions of equivalent diffraction peaks change little, implying that the lattice parameters for both compositions remain nearly constant; while for $x = 0.5$, the diffraction peaks move to the right, i.e. to higher Bragg angles, indicating that the lattice parameters $a_o$, $b_o$, $c_o$ of the orthorhombic $La_{0.5}Pr_{0.5}MnO_{3+\delta}$ are smaller than those of $La_{0.8}Pr_{0.2}MnO_{3+\delta}$ and $La_{0.7}Pr_{0.3}MnO_{3+\delta}$.

### 3.3. *TEM observations of the $La_{1-x}Pr_xMnO_{3+\delta}$ series*

Although the $La_{1-x}Pr_xMnO_{3+\delta}$ with $x = 0.2$, 0.3 and 0.5 share the same orthorhombic structure, the microstructures in $La_{0.8}Pr_{0.2}MnO_{3+\delta}$, whose magnetic

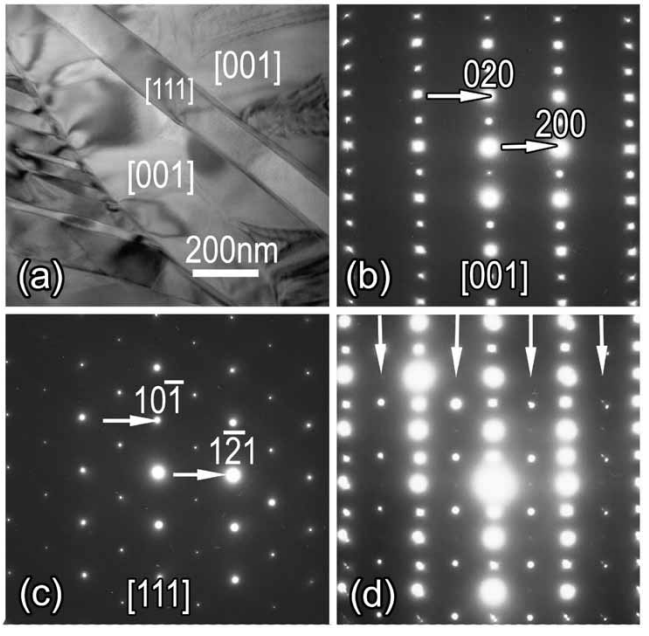


Figure 3. (a) Typical bright-field TEM image showing the morphology of bulk $La_{0.8}Pr_{0.2}MnO_{3+\delta}$. (b) and (c) [001] and [111] EDPs obtained from variant areas as marked in (a). (d) Composite EDPs of [001] and [111] obtained at the interface of these two domains, the weaker spots as marked with downward arrows are from [111] EDP. The two domains have crystallographic orientation relationship as $(010)_1//(10\bar{1})_2$, $(100)_1//(1\bar{2}1)_2$ and $[001]_1//[111]_2$.

property differs from that of the other two, are remarkably different. Figure 3a is a typical bright-field TEM image showing the morphology of bulk $La_{0.8}Pr_{0.2}MnO_{3+\delta}$. It is seen that there are highly dense stacking faults and oriented domains, which is further confirmed by selected-area electron diffraction patterns (EDPs). Figures 3b and c are [001] and [111] EDPs obtained from variant areas as marked in figure 3a. Figure 3d is a composite of EDPs of [001] and [111] obtained at the interface of these two domains. It is seen that the strong spots in these two EDPs overlap and the weaker spots, as marked with downward arrows in figure 3c, are from [111] EDP. The two domains have crystallographic orientation relationship $(010)_1//(10\bar{1})_2$), $(100)_1//(1\bar{2}1)_2$and $[001]_1//[111]_2$. Detailed analysis on the EDPs shows that there are streakings around the diffraction spots as seen in figure 3b, which implies that planar defects such as stacking faults are of high density in the $La_{0.8}Pr_{0.2}MnO_{3+\delta}$.

An extensive observation in the $La_{0.8}Pr_{0.2}MnO_{3+\delta}$ sample shows that, besides the above two domains, another oriented domain is also identified by means of electron diffraction. Figure 4a shows a configuration of the three oriented domains whose boundaries are indicated with arrows. The viewing directions are $[10\bar{1}]_1$, $[101]_2$ and $[010]_3$, respectively. Figure 4b is a composite of EDPs of $[10\bar{1}]_1$ and $[101]_2$, and figure4(c) is a composite of EDPs of $[10\bar{1}]_1$ and $[010]_3$.

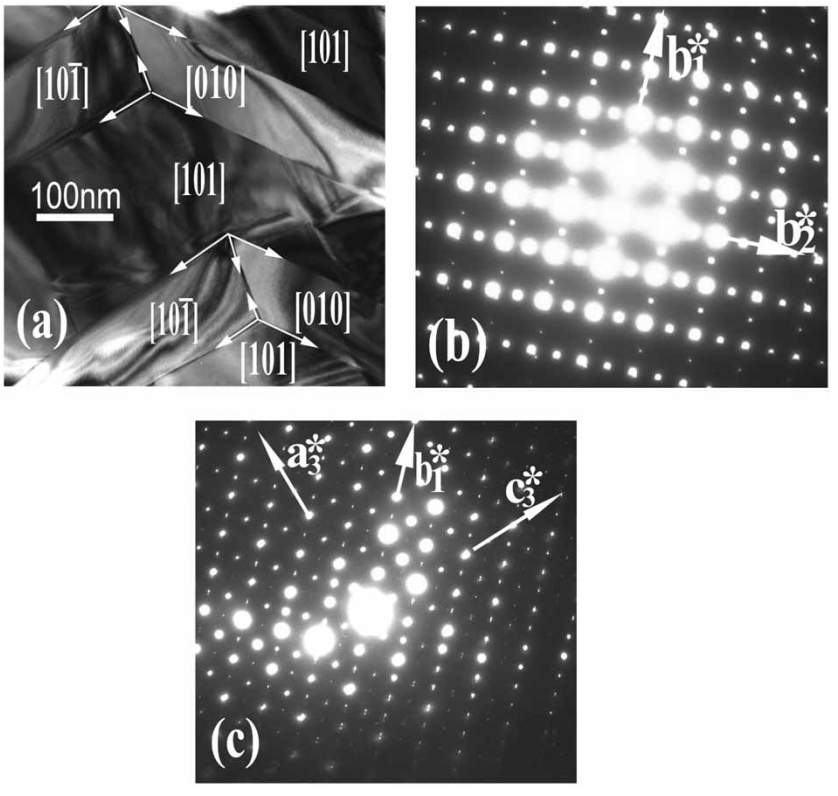


Figure 4. (a) Configuration of the three oriented domains whose boundaries are indicated with arrows. The viewing directions are $[10\bar{1}]_1$, $[101]_2$ and $[010]_3$, respectively. (b) Composite EDPs of $[10[10\bar{1}]_1$ and $[101]_2$. (c) Composite EDPs of $[10\bar{1}]_1$ and $[101]_2$.

Figure 5 shows another microstructural feature in bulk $La_{0.8}Pr_{0.2}MnO_{3+\delta}$ in which twin contrast and the contrast variation arising from the domains intersection are visible. The regular twinning below the temperature of a ferroelastic structural phase transition is a result of energy minimization. Homogeneous elastic energy in this system is reduced at the expense of twin wall energy.

Compared with the complicated microstructural configuration in bulk $La_{0.8}Pr_{0.2}MnO_{3+\delta}$, the microstructures in bulk $La_{0.7}Pr_{0.3}MnO_{3+\delta}$ and $La_{0.5}Pr_{0.5}MnO_{3+\delta}$ are quite plain. Both of them consist of large oriented domains with straight boundaries. Figure 6a is a low-magnification TEM image showing the typical microstructural features in the bulk $La_{0.7}Pr_{0.3}MnO_{3+\delta}$, in which one can see that the domain dimensions are quite large compared with that in $La_{0.8}Pr_{0.2}MnO_{3+\delta}$. Figure 6b is the [001] EDP corresponding to the upper right area in figure 6a. Figure 6c is composite of EDPs of $[001]_1$ and $[111]_2$. Neither highly dense microdomains nor twins are observed in this sample. The microstructures in $La_{0.5}Pr_{0.5}MnO_{3+\delta}$ are similar to those in $La_{0.7}Pr_{0.3}MnO_{3+\delta}$, where oriented domains are found to form straight boundaries. The experimental results in the present study are consistent with the observations of Wang *et al*. [22] in the study of

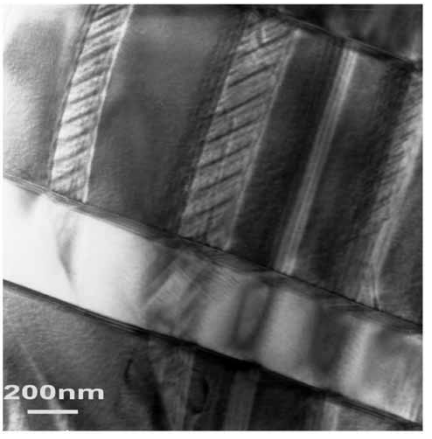


Figure 5. Another microstructural feature in bulk $La_{0.8}Pr_{0.2}MnO_{3+\delta}$ in which twin contrast and the contrast variation due to the domains' intersection are visible.

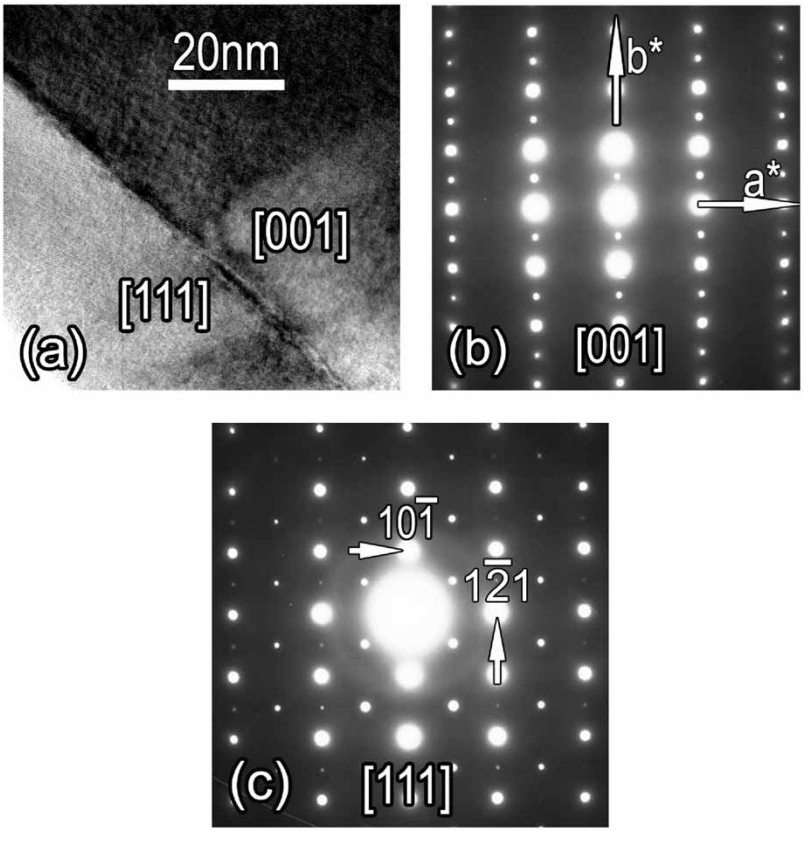


Figure 6. (a) Low-magnification TEM image showing the typical microstructural features in bulk $La_{0.7}Pr_{0.3}MnO_{3+\delta}$, in which one can see that the domain dimensions are quite large

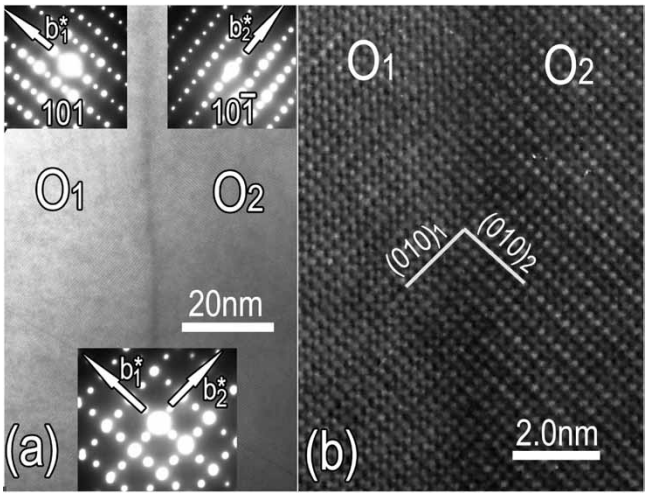


Figure 7. (a) Straight boundary of two domains in $La_{0.5}Pr_{0.5}MnO_{3+\delta}$, in which the symbols $O_1$ and $O_2$ represent oriented domains 1 and 2, respectively. Insets are EDPs corresponding to each specific area. (b) HRTEM image taken at the interface between these two domains, in which one can see that $(010)_1$ is perpendicular to $(010)_2$. Their boundary is so straight that the two domains are twinned with each other.

$La_{0.33}Ca_{0.67}MnO_3$. Figure 7a shows the straight boundary of two domains in $La_{0.5}Pr_{0.5}MnO_{3+\delta}$, in which symbols $O_1$ and $O_2$ represent oriented domain 1 and domain 2, respectively. Electron diffraction patterns corresponding to each specific area are shown as inset. Figure 7b is an HRTEM image taken at the interface between these two domains, in which one can see that $(010)_1$ is perpendicular to $(010)_2$. Their boundary is so straight that the two domains are twinned with each other.

The formation of domain structures is a consequence of a transformation from a high-symmetry phase at high-temperature to a low-symmetry phase at low temperature. In the present study, the orthorhombic oriented domains are the product of phase transformation. Owing to local and inhomogeneous stresses, which can have a different origin, such as inhomogeneous cooling, inhomogeneous composition, etc., these domains show irregular configurations, as presented in figure 5. The fact that the domains have straight boundaries and are free from microtwinning in $Pa_{0.7}Pr_{0.3}MnO_{3+\delta}$ and $La_{0.5}Pr_{0.5}MnO_{3+\delta}$ may imply that the microstructure is also affected by the Pr doping level.

## 4. Conclusions

We have studied the magnetic, structural and microstructural properties of bulk $La_{1-x}Pr_xMnO_{3+\delta}$ ($x = 0.2$, 0.3, 0.5). We found that, at low temperatures, the lower doped $La_{0.8}Pr_{0.2}MnO_{3+\delta}$ exhibits remarkable magnetic behaviour compared with

$Pa_{0.7}Pr_{0.3}MnO_{3+\delta}$ and $La_{0.5}Pr_{0.5}MnO_{3+\delta}$. Although all three compounds share an orthorhombic lattice, a salient feature in the ferromagnetic $La_{0.8}Pr_{0.2}MnO_{3+\delta}$ is the configuration of highly dense oriented domains, which may cause the pinning of magnetic walls and, thus, induce the different magnetic feature.

## Acknowledgements

The author would like to thank Professor Z. D. Zhang of the Magnetism and Magnetic Materials Division of this laboratory for stimulating discussions. Financial support with Grant Nos. 50325101 and 2002CB613503 are gratefully acknowledged.



## References

[1] R.M. Kusters, J. Singleton, D.A. Keon, *et al*., Physica B **155** 362 (1989).
[2] R. Von Helmolt, J. Wecker, B. Holzapfel, *et al*., Phys. Rev. Lett. **71** 2331 (1993).
[3] K. Chabara, T. Ohno, M. Kasai, *et al*., Appl. Phys. Lett. **63** 1190 (1993).
[4] S. Jin, T.H. Tiefel, M. McCormack, *et al*., Science **264** 413 (1994).
[5] P. Raychaudhuri, S. Mukherjee, A.K. Nigam, *et al*., J. Appl. Phys. **86** 5718 (1999).
[6] A.P. Ramirez, J. Phys. Condens. Matter **9** 8171 (1997).
[7] Y. Tomioka, A. Asamitsu, Y. Moritomo, *et al*., Phys. Rev. Lett. **74** 5108 (1995).
[8] Y. Tomioka, A. Asamitsu, H. Kuwahara, *et al*., Phys. Rev. B **53** R1689 (1996).
[9] C.N.R. Rao, R. Mahesh, A.K. Raychaudhuri, *et al*., J. Phys. Chem. Solids **59** 487 (1998).
[10] J.F. Mitchell, D.N. Argyriou, C.D. Potter, *et al*., Phys. Rev. B **54** 6172 (1996).
[11] O.I. Lebedev, G. Van Tendeloo, S. Amelinckx, *et al*., Phil. Mag. A **81** 797 (2001).
[12] H.W. Zandbergen, J. Jansen, S. Freisem, *et al*., Phil. Mag. A **80** 337 (2000).
[13] X.L. Ma, Y.L. Zhu, X.M. Meng, *et al*., Phil. Mag. A **82** 1331 (2002).
[14] Y.L. Zhu, X.L. Ma, D.X. Li, *et al*., Mater. Lett. **58** 1485 (2004).
[15] T.K. Nath, R.A. Rao, D. Lavric, *et al*., Appl. Phys. Lett. **74** 1615 (1999).
[16] A. Asamitsu, Y. Moritomo, R. Kumai, *et al*., Phys. Rev. B **54** 1716 (1996).
[17] P. Duan, Z.H. Chen, S.Y. Dai, *et al*., Appl. Phys. Lett. **84** 4741 (2004).
[18] E. Pollert, S. Krupicka and E. Kuzmicova, J. Phys. Chem. Solids **43** 1137 (1982).
[19] Private discussions with Professor Z.D. Zhang (2006).
[20] G. Matsumoto, J. Phys. Soc. Jpn. **29** 615 (1970).
[21] Y. Tokura, *Colossal Magnetoresistive Oxides* edited by Y. Tokura (Gordon and Breach, New York, 2000).
[22] R.H. Wang, J.N. Gui, Y.M. Zhu, *et al*., Phys. Rev. B **63** 144106 (2001).